Climate-related uncertainties in urban exposure to sea level rise and storm surge flooding: a multi-temporal and multi-scenario analysis

Yang Ju[a,*], Sarah Lindbergh[a], Yiyi He[a], John D. Radke[a,b]

[a] *Department of Landscape Architecture and Environmental Planning, University of California Berkeley, United States of America*
[b] *Department of City and Regional Planning, University of California Berkeley, United States of America*

ABSTRACT

Climate change-induced sea level rise and intensified storms pose emerging flood threats to global coastal urban areas. While such threats have been mapped, their uncertainties from different climate scenarios and longer planning horizons have yet to be addressed from both an exposure assessment and a stakeholder outreach perspective. Therefore, we chose the highly urbanized San Francisco Bay Area as an example to project its flood areas every 20 years between 2000 and 2100, under 24 varied climate scenarios with two greenhouse gas (GHG) concentration levels. We then assessed flood exposure by intersecting the flood areas with demographic and socioeconomic distributions, developed areas, lifeline infrastructures, and emergency responders in low elevation (< 10 m) coastal zones. Our median estimates under the low GHG scenarios indicated that 10–38% of the items assessed above are flood-exposed in 2000–2020, with this exposure increasing to 20–54% during 2080–2100. The median estimates under the high GHG scenarios for the same periods are 0–35% and 40–67%, respectively. The expected uncertainties, or standard deviations, of the exposures for a given item assessed above under the low and high GHG scenarios are 1–2% in 2000–2020 and 7–10% in 2080–2100. Despite our modeling capability for a range of climate scenarios over the long term, some stakeholders, particularly those in the private sector, prefer near-term results with lower uncertainties. This implies the need for coastal urban areas to cope with climate-related uncertainties and to focus on the long term when developing strategies and policies for climate change adaptation.

1. Introduction

The interaction between environmental hazards, urbanization, and climate change is likely to put more people and assets at risk. Environmental hazards affect urban areas and the well-being of their residents through storms, floods, heat waves, and drought (Hunt & Watkiss, 2010). At the same time, urbanization, particularly disorderly urbanization, is increasingly exposing urban areas to these hazards (Dawson et al., 2011; Pelling, 2003; Storch & Downes, 2011). This urban-hazard interaction alters under climate change which increases the extent, frequency, and severity of current-day environmental hazards, eventually affecting urban areas that were not previously exposed. To mitigate these undesirable consequences, cities have addressed environmental hazards and climate change issues in their master, strategic, and action plans (Jabareen, 2015). Researchers have also modeled the impact of climate change and environmental hazards on different population groups (Bickers, 2014; Kaźmierczak & Cavan, 2011; KC, Shepherd, & Gaither, 2015; Martinich, Neumann, Ludwig, & Jantarasami, 2013; Nutters, 2012), infrastructures (Biging, Radke, & Lee, 2012; Demirel, Kompil, & Nemry, 2015; Radke et al., 2018, 2017), and natural environments (Schile et al., 2014; Zhu, Xi, Hoctor, & Volk, 2015). The modeled impacts can also be used to facilitate public participation in adaptation planning (Wadey et al., 2015).

Coastal urban areas are likely to have intensified flood threats from storm surge and sea level rise (SLR) while simultaneously experiencing increasing development pressure, and thus should be prioritized for climate change adaptation (Carter et al., 2015; Rosenzweig, Solecki, Hammer, & Mehrotra, 2010). Due to their access to water, maritime transportation, fertile soil, raw materials - including salt and sand, and tourist attractions, coastal zones have been hotspots for development and population growth (Creel, 2003; De Sherbinin, Schiller, & Pulsipher, 2007; UNU-IHDP, 2015). A 2007 assessment indicated that while low elevation (i.e. < 10 m above sea level) coastal zones only covered 2% of the world's land area, they contained 10% of the world's population and 13% of the world's urban population (McGranahan, Balk, & Anderson, 2007). A global meta-analysis of 292 locations found

that the average urban expansion rate in low elevation coastal zones between 1970 and 2000 was > 5.7%, higher than the rate of all other areas combined (Seto, Fragkias, Güneralp, & Reilly, 2011). Coastal zones are growth hotspots for the future: a conservative projection estimates that the global population in low elevation coastal zones will increase by 50% between 2000 and 2030, and by > 160% between 2000 and 2060 (Neumann, Vafeidis, Zimmermann, & Nicholls, 2015). Such high concentration of population and assets explain why coastal urban areas are more vulnerable to flood hazards from SLR and storm surge than other areas (Hunt & Watkiss, 2010).

Studies have modeled flooding from SLR and storm surge and analyzed the exposure of coastal areas (Barnard et al., 2009, 2014; Biging et al., 2012; Dasgupta, Laplante, Meisner, Wheeler, & Yan, 2008; Knowles, 2009, 2010; Lang, Radke, Chen, & Chan, 2016; Marcy et al., 2011; Radke et al., 2017; Schile et al., 2014; Strauss, Ziemlinski, Weiss, & Overpeck, 2012). A typical approach in these studies is to produce and utilize flood maps under different storm recurrence intervals (e.g. 10-year and 100-year) combined with generic, incremental SLR values that are not closely associated with specific climate scenarios and planning horizons. While this generic approach provides the flexibility to adapt itself to various and continuously updating climate projections, it may lack the specificity to show what the flooding is like under specific climate scenarios and planning horizons that stakeholders are interested in, as well as the uncertainty introduced by different climate scenarios and how the uncertainty propagates over time.

To show the uncertainty in long-term flood projections under climate change, and to discuss the implications of such uncertainty in planning and management for climate change adaptation, we conducted flood simulations that incorporated SLR and storm surge to identify a coastal urban area's flood exposures under a range of 24 different climate scenarios at two greenhouse gas (GHG) concentration levels, every 20 years between 2000 and 2100. We measured flood exposures by intersecting the simulated flood with demographic and socioeconomic distributions, developed areas, lifeline infrastructures, and emergency responders. Uncertainties were further calculated as standard deviations of those flood exposures.

We focus on the San Francisco Bay Area (Bay Area), a major U.S. urban area in the State of California, in this study. The Bay Area is a prime candidate for this research as it is prone to flooding from SLR and intensified storms induced by climate change, and it has a large concentration of development in threatened low-lying coastal areas (Fig. 1). The Bay Area contains major U.S. urban agglomerations including San Francisco, Oakland, and the Silicon Valley complex centered in San Jose. This area continues to rapidly expand due to a growing economy and employment opportunities. Population, jobs, households and housing units in the Bay Area are projected to increase by 24–30% between 2010 and 2040, introducing new demands for land development (The Association of Bay Area Governments (ABAG), Metropolitan Transportation Commission (MTC), 2013). Due to the demand for land development and insufficient regulations, the Bay Area's coastal zones have been transforming rapidly from their natural state into industrial and residential use located at or below sea level (Pinto & Kondolf, 2016). As a result, the Bay Area's exposures to potential flooding from storm surge and SLR have increased. A 2012 study shows that a 1 m SLR combined with a 100-year storm will put 220,000 people at risk and cost 49 billion US dollars to replace the impacted property, and that a 1.4 m SLR will increase the numbers to 270,000 and 62 billion US dollars (Heberger, Cooley, Moore, & Herrera, 2012).

Taken together, our primary goal is to illustrate the uncertainty in long-term projection of urban exposure to climate change-induced flooding. To achieve this goal, we first provide comprehensive mapping of flood hazard and exposures of urban areas under different climate scenarios and time horizons. Second, we highlight how the exposure's uncertainties change with time and vary by groups of the climate scenarios defined by their GHG levels. In addition, we discuss the uncertainties' implications in planning and management based on our outreach process with stakeholders. Through these efforts, we highlight the necessity of understanding climate-related uncertainties in coastal flood projections and exposure analysis. We also reveal some challenges for stakeholders in utilizing multi-scenario and long-term climate and environmental hazard projections in planning, management, and decision-making. While we focus on the Bay Area and coastal flooding, our findings are informative for other coastal urban areas faced with similar flood threats, and for adaptation to other climate change-induced environmental hazards (e.g. drought and heatwave) whose uncertainties are intrinsic and substantially larger in the longer term.

2. Data and methods

2.1. Flooding model

Various models, both static and dynamic, have been used to simulate coastal flood. Earlier models tend to be static, identifying flood areas below a time-invariant water surface such as the projected mean sea level. These static models are computationally feasible, therefore can be applied to large areas with fine spatial resolutions (Biging et al., 2012; Dasgupta et al., 2008; Marcy et al., 2011; Strauss et al., 2012). However, these models do not incorporate the temporal and flow dynamics of water movement. More recent research has employed process-based, hydrodynamic, two-dimensional (2D) models to account for these dynamics. These 2D models are computationally intensive, and thus difficult to implement at regional scales and/or with fine spatial resolutions. Few studies, including the model by Knowles (2009, 2010), the Coastal Storm Modeling System (CoSMoS) (Barnard et al., 2009, 2014), and the CalFloD-3D model (Radke et al., 2017), adopted 2D hydrodynamic models for the Bay Area.

We employed a 3Di hydrodynamic model (Stelling, 2012) to simulate flood areas and depth at 50 m spatial resolution during extreme sea level events projected under a range of 24 climate scenarios defined by two greenhouse gas (GHG) concentration levels, every 20 years between 2000 and 2100. The 3Di model dynamically simulates the movement of water, by user-defined time steps, over a digital surface of topography and bathymetry. This model has been successfully implemented in urban and rural watersheds to simulate flood by inland rainfall-runoff (Dahm, Hsu, Lien, Chang, & Prinsen, 2014; Hsu, Prinsen, Bouaziz, Lin, & Dahm, 2016; Leicher, 2016), SLR, and storm surge (Ju et al., 2017; Radke et al., 2017). The 3Di model's primary inputs are time-series water levels as boundary forcing to generate waterflows, and digital surface data containing topography, bathymetry, and/or aboveground objects such as levees to direct the waterflows. For every extreme sea level event, the 3Di model produces a time-series of flood areas with water depths. A unique advantage of the 3Di model for this study is its ability to feasibly compute over large regions at fine spatial resolutions, which is enabled by the model's compression algorithm that simplifies the input digital surface while preserving significant topographic variations such as those from levees and buildings (Stelling, 2012). In this study, we modeled at 50 m spatial resolution to feasibly iterate through the various extreme sea level events.
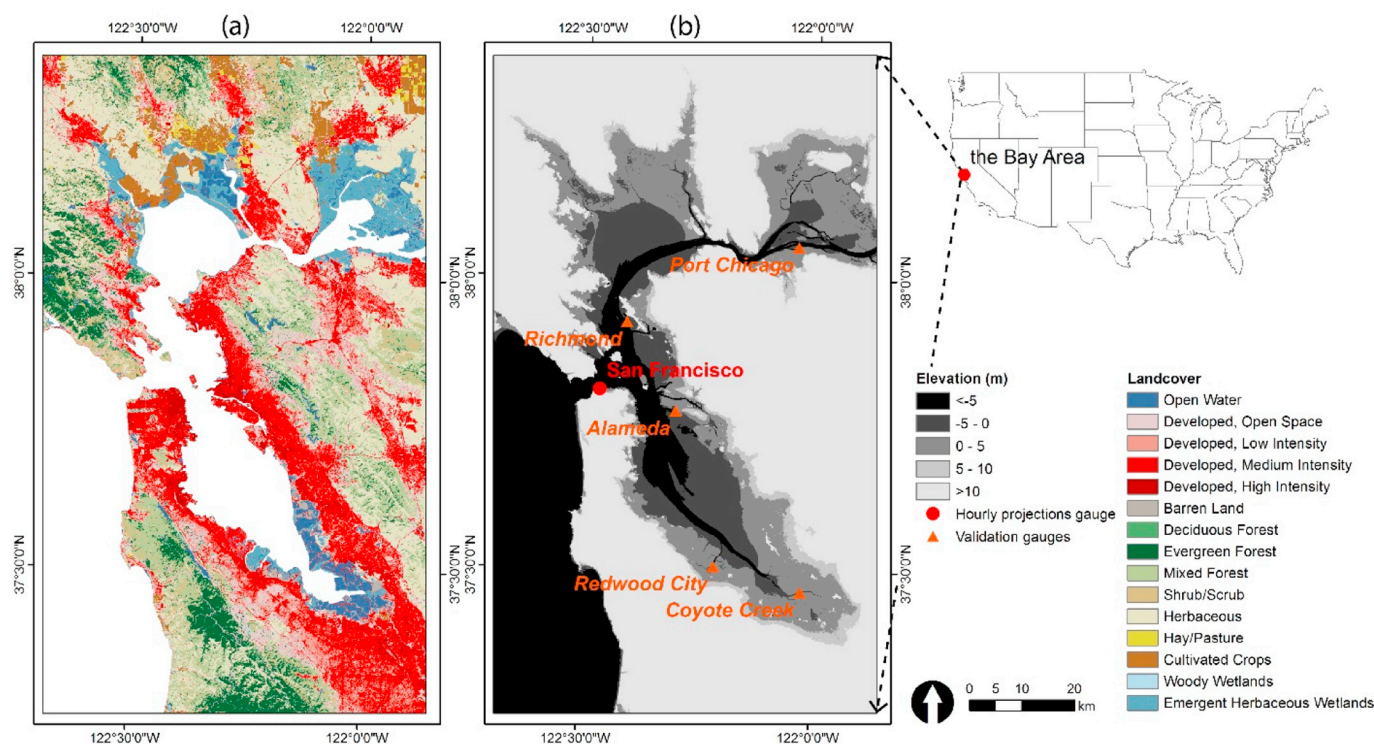
Fig. 1. The San Francisco Bay Area. (a) shows the Bay Area's landcover types in 2011, and (b) shows its elevation with areas below 10 m highlighted in darker tones, the gauge with the hourly sea level projections, and the validation gauges used for flood model calibration.

2.2. Extreme sea level events

We used extreme sea level events to simulate the worst-case flood hazards with the 3Di model. These extreme sea level events were extracted from an hourly sea level projection (Cayan, Kalansky, Iacobellis, & Pierce, 2016) at a San Francisco gauge (Fig. 1) and incorporated long-term SLR and short-term fluctuations from tide and storm surge. Each event is a 72-h window starting with the highest sea level under a given climate scenario during a 20-year period between 2000 and 2100 (Fig. 2(a)). The events together represent a spectrum of 24 climate scenarios generated from a hierarchy of two Representative Concentration Pathways (RCPs) defining low and high atmospheric concentrations of GHG (i.e. RCP 4.5 versus 8.5), three probabilistic SLR values, and four Global Climate Models (GCMs) emphasizing different historical and future climate patterns in California (Pierce, Cayan, & Dehann, 2016) (Fig. 2(b)). For each RCP and a 20-year period, we ranked the corresponding twelve extreme sea level events by their peak sea levels to derive high, medium, and low estimates of flood hazard. We used the 20-year intervals to match the simulated flood and exposure analysis with typical planning horizons and investment cycles that were often multidecadal. It is worth noting that the climate scenarios, our flood projections, and exposure analysis are intended to show a wide range of plausible futures and not to predict an exact one (Moss et al., 2010).

The extreme sea level events show higher and increasingly varied peak sea levels as the events move into the future (Fig. 3). Under RCP 4.5 scenarios, the peak sea level reaches 2.61–2.94 m during the 2000–2020 period, and 3.08–4.40 m during the 2080–2100 period. Under RCP 8.5 scenarios, the numbers shift to 2.49–2.63 m during the

2000–2020 period, and 3.78–5.50 m during the 2080–2100 period. The peak sea levels under RCP 8.5 tend to be higher than those under RCP 4.5, which is likely due to RCP 8.5's higher GHG concentrations, stronger climate change, greater SLR, and more intensified storms (see Appendix A for a visualization of the hourly sea level projections, SLR, and storm surge). However, during the 2000–2020 period, RCP 4.5 scenarios project higher peak sea levels than RCP 8.5 scenarios, which is due to stronger storm surge projections by one GCM under RCP 4.5 scenarios (Appendix A). The variability of the peak sea levels exacerbates over time, for example, increasing from 0.14 m (i.e. 2.63 m versus 2.49 m) in the 2000–2020 period to 1.72 m (5.50 m versus 3.78 m) in the 2080–2100 period under RCP 8.5.

2.3. Topography and bathymetry data

We generated a continuous, 50 m resolution surface from the best-available topography and bathymetry datasets (Table 1) of the Bay Area as the second input for the 3Di model. Our surface contains bare ground elevation, bathymetry, and levees. We excluded buildings as they were too granular for the 50 m resolution surface. Since the datasets are originally all finer than the targeted 50 m spatial resolution, we first conducted an average aggregation and then mosaicked the aggregated datasets to generate the 50 m resolution surface. Flood control structures, such as levees, have their elevation information preserved to some extent in the 50 m resolution surface. However, underestimated elevations are introduced when averaging levee segments with their lower elevation surroundings. Similarly, small channels protected by extensive levees can have overestimated elevations after the aggregation. Such underestimation for the levees and overestimation for the
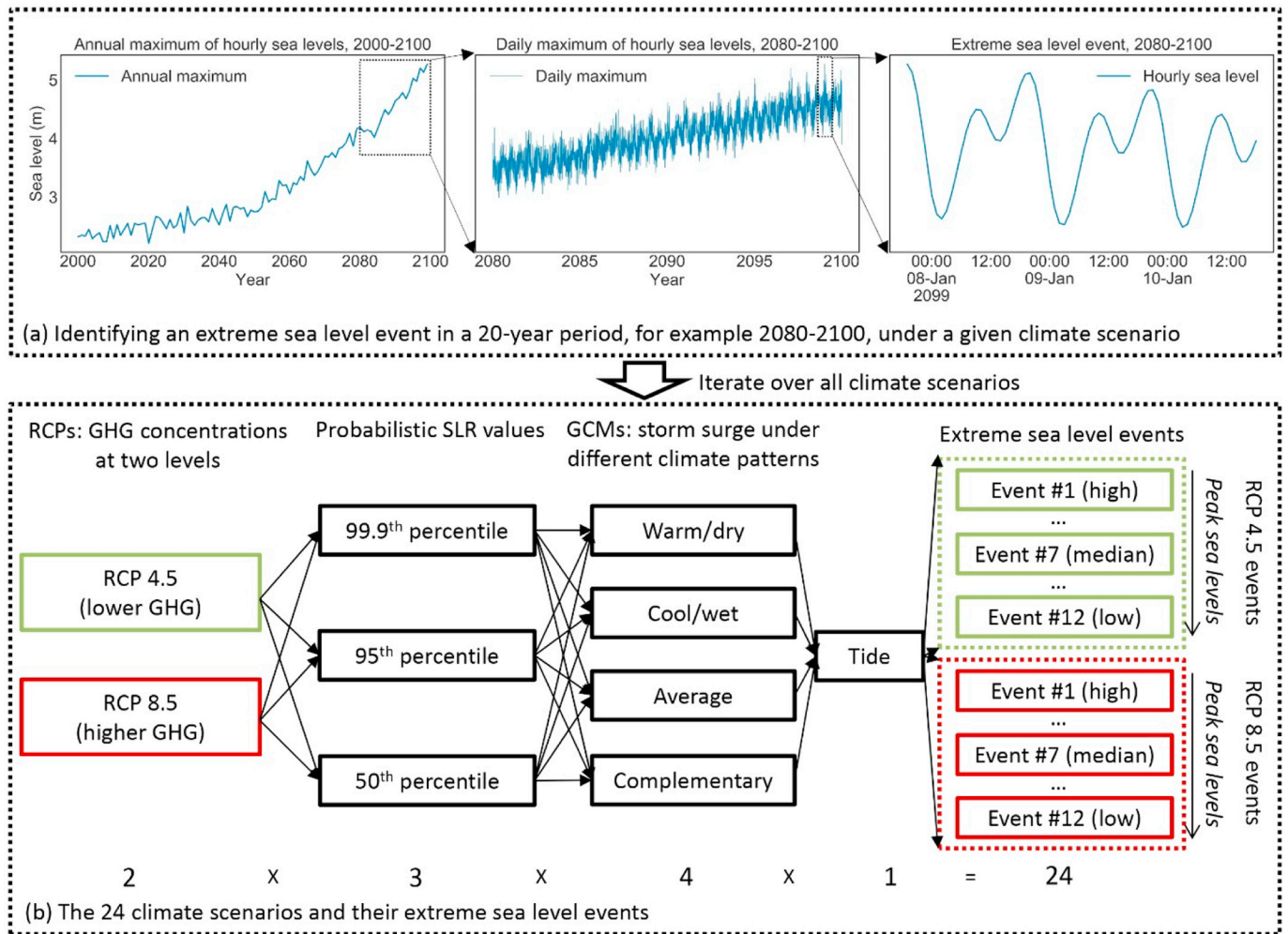
Fig. 2. The climate scenarios and their extreme sea level events. (a) shows an example of extracting an extreme sea level event for a 20-year period and a given climate scenario from the hourly sea level projections. This extreme sea level event is a 72-h period started with the highest sea level projected under this climate scenario and during this 20-year period. (b) shows the hierarchy to generate the climate scenarios and ranking of the extreme sea level events by their peak sea levels.
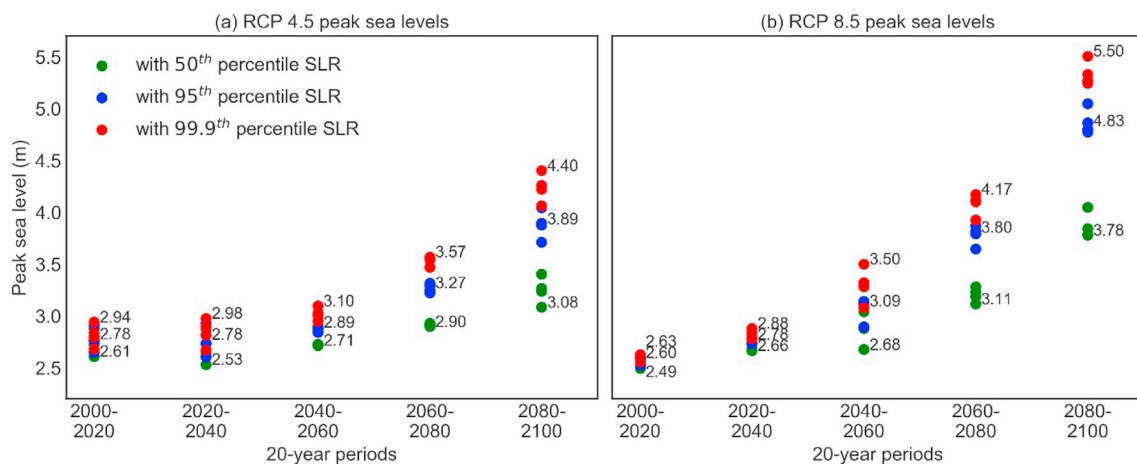

Fig. 3. Projected peak sea levels during the extreme sea level events at the San Francisco gauge. Each dot represents the peak sea level under a climate scenario generated from permutations of two RCPs, three problablistic SLRs, and four GCMs during a 20-year period. The maximum, median, and minimum estimates of peak sea levels for an RCP and a 20-year period are labeled. The colors differentiate the three probabilistic SLRs generating the peak sea levels. (a) shows the peak sea levels under RCP 4.5 scenarios, and (b) shows the peak sea levels under RCP 8.5 scenarios.

Table 1
Topography and bathymetry datasets used to construct the 50 m surface.

Data	Spatial resolution	Spatial coverage	Use in the 50 m surface	Source
USGS South Bay Lidar NOAA North Bay Lidar	1 m	Low elevation coastal zones	Fine resolution topography	USGS California Coastal LiDAR Project (https://coast.noaa.gov/htdata/lidar1_z/geoid12a/data/1406/) NOAA California Coastal LiDAR Project (https://coast.noaa.gov/htdata/lidar1_z/geoid12a/data/584/)
National Elevation Dataset (NED)	10 m	The entire Bay Area	Supplementary topography to finer resolution datasets	USGS National Elevation Dataset (https://lta.cr.usgs.gov/NED)
DWR Bay-Delta bathymetry	2–10 m	The entire Bay Area	Fine resolution bathymetry	California Department of Water Resources (https://www.sciencebase.gov/catalog/item/58599681e4b01224f329b484)

small channels can either generate non-existent water flow pathways or eliminate existing ones. Therefore, the 50 m resolution surface can over- or underestimate flooding. However, we used the average aggregation (versus maximum or minimum aggregation) as it showed an average condition of the topography. Interested researchers may further test the effects of other aggregation methods on the simulated floods.

2.4. Model validation and representation of flood hazard

We modeled a historical high sea level event on Jan 11th, 2017 in the Bay Area (NOAA, 2019) to validate the model's settings before iteratively simulating through the extreme sea level events identified in Section 2.2. We compared the simulated water levels against observations at five validation gauges in Fig. 1. The results (Fig. 4) show that the model simulates similar water levels to the historical event, with Pearson correlation coefficient (r, calculated with Eq. (1)) between the simulations and the observations ≥ 0.81 and root mean square error (RMSE, calculated with Eq. (2)) ≤ 0.69 m, when no time lag between the simulations and observations is applied to calculating correlation and RMSE. The difference between the observations and the simulations increases when moving inland, with it being smaller for the near coast Alameda gauge ($r = 0.92$, RMSE = 0.31 m) and greater for inland gauges such as Port Chicago ($r = 0.81$, RMSE = 0.57 m) and Coyote Creek ($r = 0.82$, RMSE = 0.69 m). Overall, the simulations tend to underestimate the observations, which can be explained by the absence of river discharges that affect water levels in the simulations. We also notice time lags between the simulations and the observations, as a certain amount of time is required for the simulated waterflows to pass through the gauges and to alter the initial water surface of 0 m in elevation. When an arbitrary 30-min lag was added to comparing the observations and the simulations, the differences reduced for all gauges, and the lowest correlation increased from 0.81 (without lag) to 0.90 (with lag) and the highest RMSE reduced from 0.69 m (without lag) to 0.54 m (with lag). The existence of such time lags justifies the need for simulating the extreme sea level events over longer time windows (e.g. 72 h), so that the simulated water peaks can pass through the study area.

$$r = \frac{\sum_{t=1}^{n} (x_t - \overline{X})(\widehat{x_t} - \overline{\widehat{X}})}{\sqrt{\sum_{t=1}^{n} (x_t - \overline{X})^2} \sqrt{\sum_{t=1}^{n} (\widehat{x_t} - \overline{\widehat{X}})^2}} \quad (1)$$

$$RMSE = \sqrt{\frac{\sum_{t=1}^{n} (\widehat{x_t} - x_t)^2}{n}} \quad (2)$$

where x_t is the observed value at time step t, and $\widehat{x_t}$ is the simulated value, $\overline{X}$ is the average value of the observations, $\overline{\widehat{X}}$ is the average value of the simulations, n is the total number of time steps.

During each extreme sea level event our simulation produced hourly flood area and depths, which were compressed into a single map of the maximum flood extent and depth during the event. We also grouped the maps from different events by their respective RCPs and 20-year periods to show coastal flood hazard under different GHG concentration levels and over time.

2.5. Exposure analysis

We collected fourteen datasets representing demographic and socioeconomic distributions, developed areas, locations of lifeline infrastructures, and emergency responders (Table 2) to comprehensively assess the Bay Area's exposure to the projected flood. Demographic and socioeconomic data including population, number of households and housing units were used to estimate the total amount of people, families, and housing structures exposed to flooding. Similarly, developed areas of different development intensities were used to approximate the exposure of the built-environment (i.e. man-made environment ranging from dense urban centers and parks) in general (Wood, 2009). We
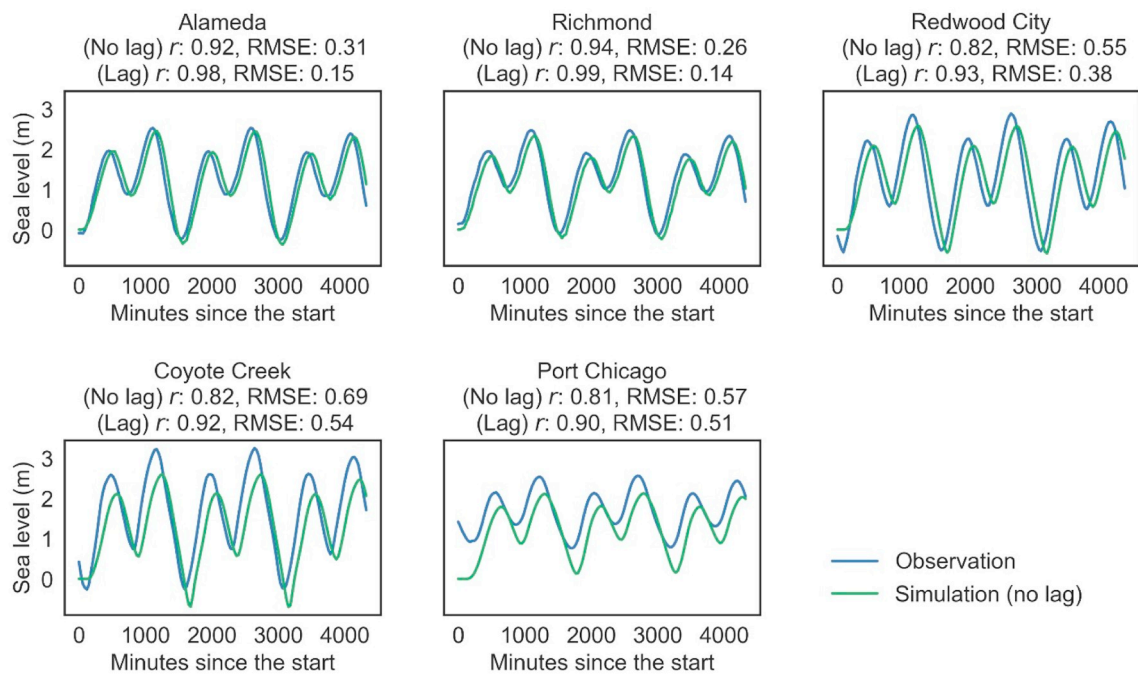
Fig. 4. Observed and simulated water levels during a historical extreme sea level event in the Bay Area starting in Jan 11th, 2017. Observations and simulations were compared using Pearson correlation coefficient (r) and root mean square error (RMSE), with and without an arbitrary 30-min time lag.

included lifeline infrastructures containing roads and co-located utilities (e.g. electric power and natural gas) as they support the recovery of places directly hit by environmental hazards, and the failure of these infrastructures can spread the hazards' impacts to a broader region (EERI, 2016; Oh, Deshmukh, & Hastak, 2013). Emergency responders, such as fire stations and hospitals, were also included in the exposure analysis due to their importance in disaster response and their abilities to assist needed citizens affected by environmental hazards (Biging et al., 2012; Coles, Yu, Wilby, Green, & Herring, 2017).

We used relative exposure, which was calculated as the percentage of a dataset's low-lying portion (i.e. < 10 m in elevation) that was flooded, in the following analysis. Calculating exposure is a preliminary step

towards understanding flooding's impact, as this measurement does not show outcomes such as monetary loss from flooded homes and infrastructures, reduced service area and capacity of emergency responders, or any cascading effects due to disruptions in lifeline infrastructures. However, this exposure metric can be easily iterated through the multiple extreme sea level events to provide an overview of the uncertainties driven by the climate scenarios and time. In addition, we focused on relative exposure to facilitate comparison across different datasets. We also limited the analysis to the low-lying portion of these datasets as coastal flooding from SLR and storm surge is a localized phenomenon that rarely expands to higher elevations. A detailed description of what relative exposure means to each dataset is contained in Table 2. In

Table 2
Datasets used in the exposure analysis.

Datasets		Source	Relative exposure metric
Demography and socioeconomics	Population	The U.S. Census Grids (http://sedac.ciesin.columbia.edu/data/collection/usgrid)	% people
	Number of households		% households
	Number of housing units		% housing units
Developed areas	Open space	National Land Cover Database (https://www.mrlc.gov/nlcd11_data.php)	% area
	Low intensity development		
	Medium intensity development		
	High intensity development		
Lifeline infrastructures	Roads	ArcGIS Business Analyst 2016 (ESRI, 2016)	% length
	Electric transmission line	GIS Open Data, California Energy Commission (https://cecgis-caenergy.opendata.arcgis.com)	% length
	Electric substations		% substations
	Natural gas pipelines		% length
	Natural gas stations		% stations
Emergency responders	Fire stations	(Biging et al., 2012)	% stations
	Hospitals	Licensed Healthcare Facility Listing, California Health and Human Services Open Data Portal (https://data.chhs.ca.gov/dataset/licensed-healthcare-facility-listing)	% hospitals

%: percentage of a dataset's low-lying portion (i.e. < 10 m in elevation) that is flooded.
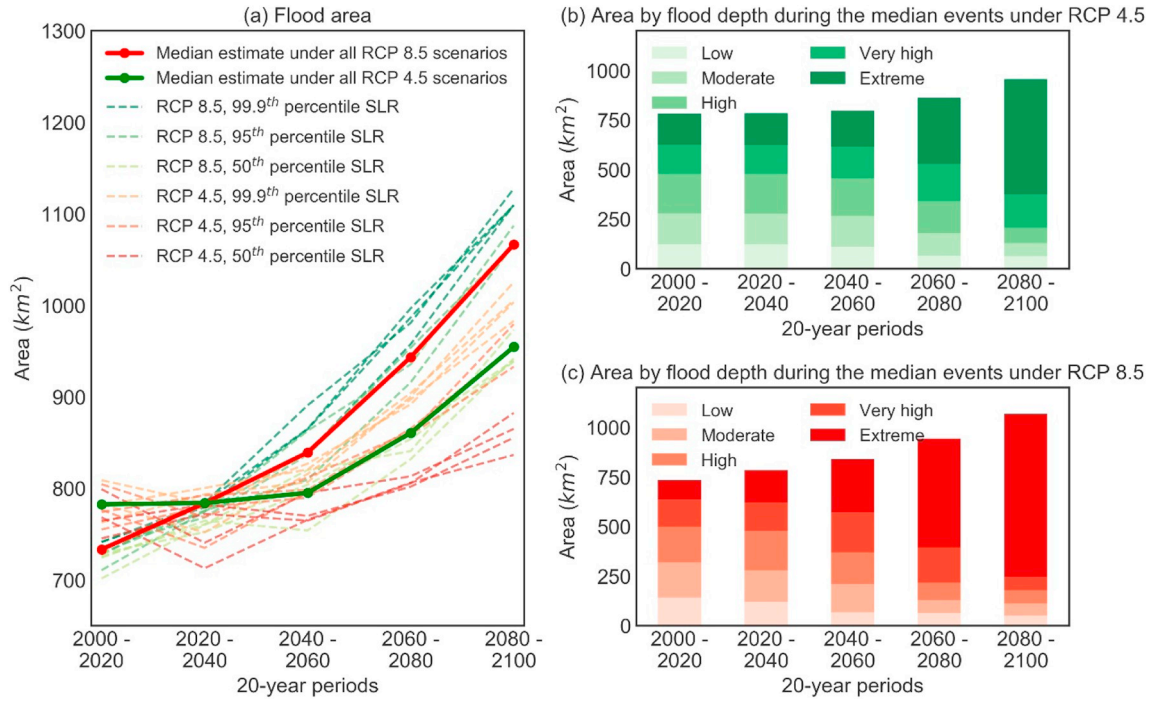
Fig. 5. Flood area during the extreme sea level events identified every 20 years between 2000 and 2100 under the 24 climate scenarios. (a) Flood area of each event, shown as dashed lines colored by their RCPs and probabilistic SLR values. The median estimate of each RCP is shown as a solid line. (b) and (c) show area with different maximum flood depths (i.e. low: 0–0.5 m, moderate: 0.5–1.0 m, high: 1.0–1.5 m, very high: 1.5–2.0 m, extreme: > 2.0 m) based on the median estimates of each RCP.

addition, we report absolute exposures of the datasets in Appendix B.

2.6. Analyzing uncertainties in the exposures

We calculated uncertainties in the exposures as standard deviation ($Std_{j, t, k}$) of a dataset's (k) relative exposures during all extreme sea level events for a given 20-year period (t) and an RCP (j) (Eq. (3)). We performed a simple linear regression to understand how these uncertainties changed with the RCPs and time (Eq. (4)). The fitted value from this regression represents expected uncertainty in relative exposures of a dataset for a RCP and a 20-year period. We calculated the uncertainties and performed the regression above for the overall exposure with the maximum flood depth > 0 m, as well as for five different levels of exposure stratified by the maximum flood depth: low (0–0.5 m), medium (0.5–1.0 m), high (1.0–1.5 m), very high (1.5–2.0 m), and extreme (> 2.0 m).

$$Std_{j,t,k} = \sqrt{\frac{\sum_{i=1}^{N}(E_{i,j,t,k} - \overline{E_{j,t,k}})^2}{N}}$$
(3)

$$Std_{j,t,k} = \beta_0 + \beta_1 RCP_j * Time_t + \varepsilon_{j,t,k}$$
(4)

where $E_{i, j, t, k}$ is a dataset k's relative exposure during an extreme sea level event i of RCP j and a 20-year period t. $\overline{E_{j,t,k}}$ is the average relative exposure across the extreme sea level events. N is the total number of extreme sea level events of RCP j and 20-year period t, which equals to 12 based on permutations of the four GCMs and three probabilistic SLR values. $Std_{j, t, k}$ is standard deviation of the dataset's relative exposures under RCP j and during 20-year period t. RCP_j is a dummy variable for

either RCP 4.5 or RCP 8.5, and $Time_t$ is a dummy variable for one of the five 20-year periods.

3. Results

3.1. Flood hazard

Our simulations of the extreme sea level events indicate that flood area and depth increase with the projected SLR and intensified storms. The median estimates of RCP 8.5 scenarios and their respective extreme sea level events show that flood area increases from 733 km² during the 2000–2020 period, to 784 km² during the 2020–2040 period, and to 1066 km² during the 2080–2100 period (Fig. 5(a), solid red line). Compared with the median estimates of RCP 8.5, the ones of RCP 4.5 scenarios results in larger flood areas during the 2000–2020 period, and smaller flood areas during the remaining periods (Fig. 5(a), solid green line). Such patterns are expected as RCP 4.5 scenarios have higher peak sea levels for the events during the 2000–2020 period but lower peak sea levels for the events during the other periods, as shown in Section 2.2. Our results also indicate that the increased portions of the flood areas have greater depth (Fig. 5(b–c)). For example, the median estimates of RCP 8.5 scenarios show 13% (97 km²) of the total flood area with extreme depth (i.e. > 2.0 m) during the 2000–2020 period, 21% (165 km²) during the 2020–2040 period, and 77% (822 km²) during the 2080–2100 period (Fig. 5(c)).

The flood areas mainly include wetlands in the north and south, and developed areas in the central section of the Bay Area. While flooding over the wetlands moves further inland, in the developed areas it is
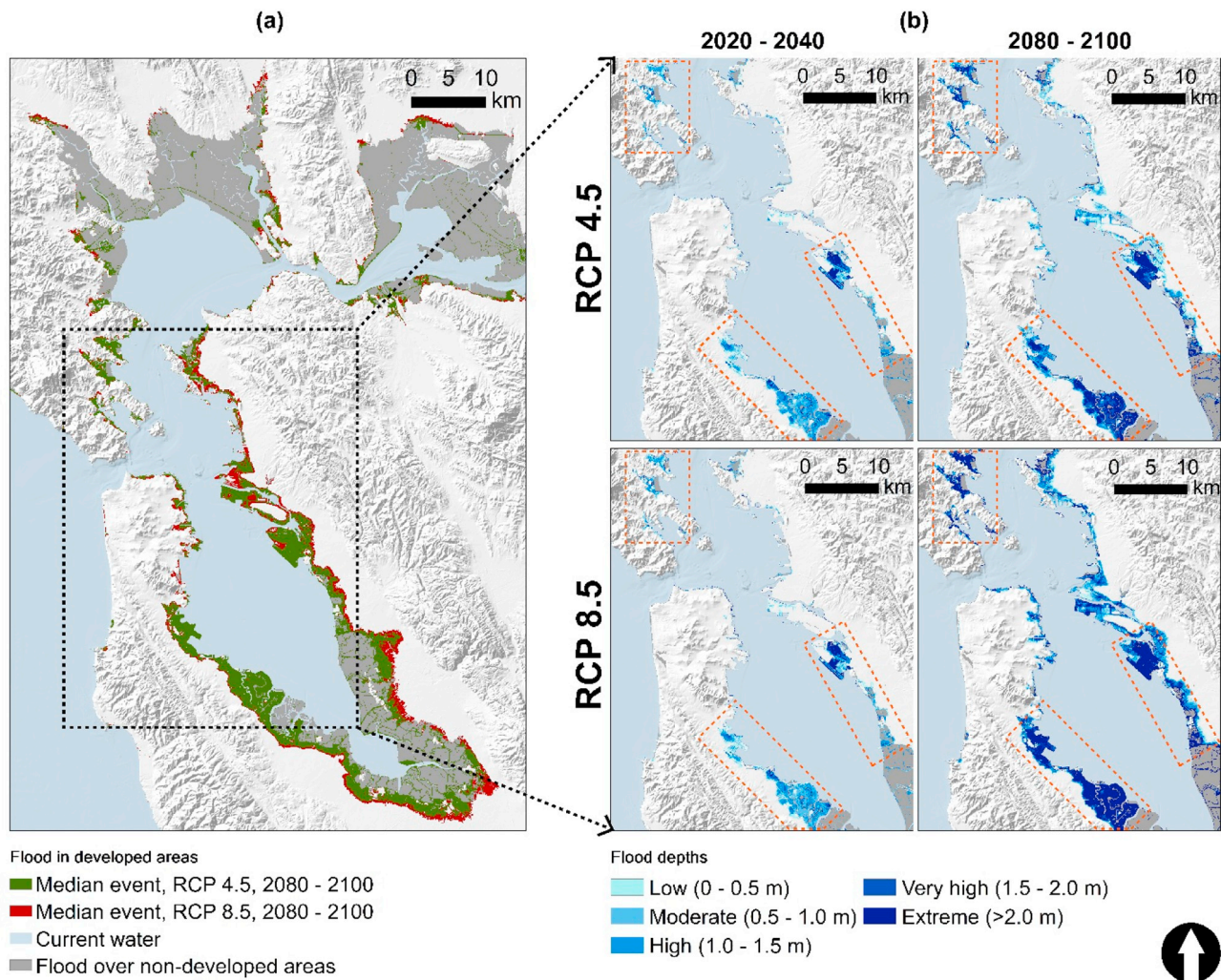
Fig. 6. Flood in developed areas based on the median estimates of RCP 4.5 and 8.5 scenarios. (a) shows overall flood area during the 2080–2100 period. (b) compares flood depths from the median estimates of the two RCPs and two 20-year periods. (b) also outlines areas with limited expansion in flood area but disproportional increases in flood depth.

constrained by steep slopes and hills (Fig. 6(a)). Due to these topographic constraints, the developed areas are likely to have limited expansions in flood area but greater increases in flood depth, which partially explains why areas with greater flood depth grew disproportionally in Fig. 5(b–c). We also visually identify several locations that will likely have disproportional increases in areas with deeper flooding in Fig. 6(b).

3.2. Urban exposure to flooding

Our results indicate that the fourteen datasets assessed are increasingly exposed to the simulated flooding and that RCP 8.5 scenarios generally cause greater exposures than do the RCP 4.5 scenarios (Fig. 7). While we report relative exposures (i.e. percentage of a dataset's low-lying portion that is flooded, see Table 2 for a detailed description for each dataset) in this study, we include absolute exposures in Appendix B.

Under the median estimates of RCP 8.5 scenarios, the fourteen datasets' relative exposures increase from 0-35% (i.e. dataset dependent, similar below) during the 2000–2020 period to 40–67% during the 2080–2100 period. Under the median estimates of RCP 4.5 scenarios, the exposures are 10–38% during of the 2000–2020 period, and 20–54% during the 2080–2100 period. Compared with RCP 4.5, RCP 8.5 does not consistently lead to more exposures of the datasets. Over the five 20-year periods combined, the median estimates of RCP 8.5 scenarios result in significantly higher (p-value = 0.038) exposures of the fourteen datasets. However, before 2040, RCP 4.5's median estimates lead to insignificantly higher exposures (p-value$_{2000–2020}$ = 0.394, p-value$_{2020–2040}$ = 0.916). After 2040, RCP 8.5 scenarios' median estimates start to cause more exposures, and such pattern becomes increasingly significant (p-value$_{2040–2060}$ = 0.368, p-value$_{2060–2080}$ = 0.036, p-value$_{2080–2100}$ = 0.000). This pattern is due to the differences in projected peak sea levels between the two RCPs, as illustrated earlier in Section 2.2.
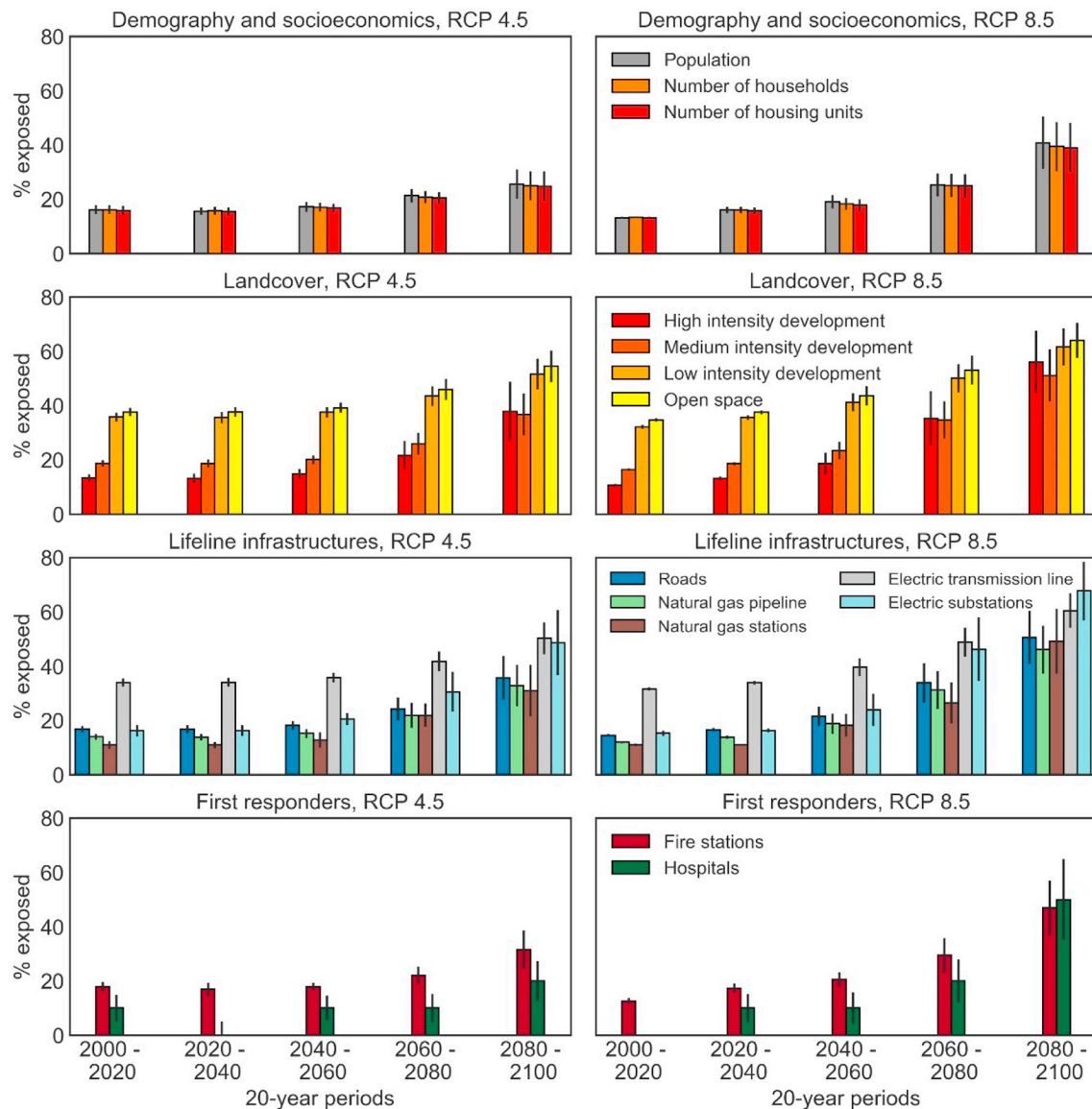
Fig. 7. Relative flood exposure of demographic and socioeconomic distributions, developed areas, lifeline infrastructures, and first responders during the extreme sea level events under RCP 4.5 and 8.5 scenarios, every 20 years between 2000 and 2010. Relative exposure is calculated as percentage of a dataset's low-lying portion (i.e. < 10 m in elevation) that is flooded. The solid color bars show the relative exposures during median estimates of the extreme sea level events. The black lines show standard deviations of the relative exposures during all extreme sea level events for a given RCP and a 20-year period.

Developed open space and low intensity development are the most exposed sub-categories on average over the 20-year periods, whereas hospitals, demographic and socioeconomic distributions are less exposed. Averaged over the median estimates during the five 20-year periods, 43% (RCP 4.5) to 47% (RCP 8.5) of developed open space and 41% (RCP 4.5) to 44% (RCP 8.5) of low intensity development within the low-lying coastal zones are exposed to flooding. The less exposed sub-categories, such as hospitals and housing units, have exposures of 12% (RCP 4.5) to 18% (RCP 8.5) and 19% (RCP 4.5) to 22% (RCP 8.5), respectively. Development is the most exposed category we assess, followed by lifeline infrastructures, demographic and socioeconomic distributions, and emergency responders.

3.3. Uncertainties driven by the climate scenarios and time

The uncertainties (i.e. standard deviations) of the datasets' relative exposures increase over time, and RCP 8.5 generally leads to more uncertainties compared with RCP 4.5 (Fig. 8). Under RCP 4.5 scenarios, the 2000–2020 period has an expected uncertainty (i.e. based on the regression of Eq. (4)) of 2% in relative exposure of a given dataset, and the uncertainty is relatively unchanged until the 2060–2080 period when the value doubles to 4%. The final 2080–2100 period has the highest expected uncertainty of 7% (Fig. 8(a)). A similar trend is found for RCP 8.5's average uncertainties, despite an earlier rise in the 2020–2040 period (Fig. 8 (b)). During the 2000–2020 and 2020–2040
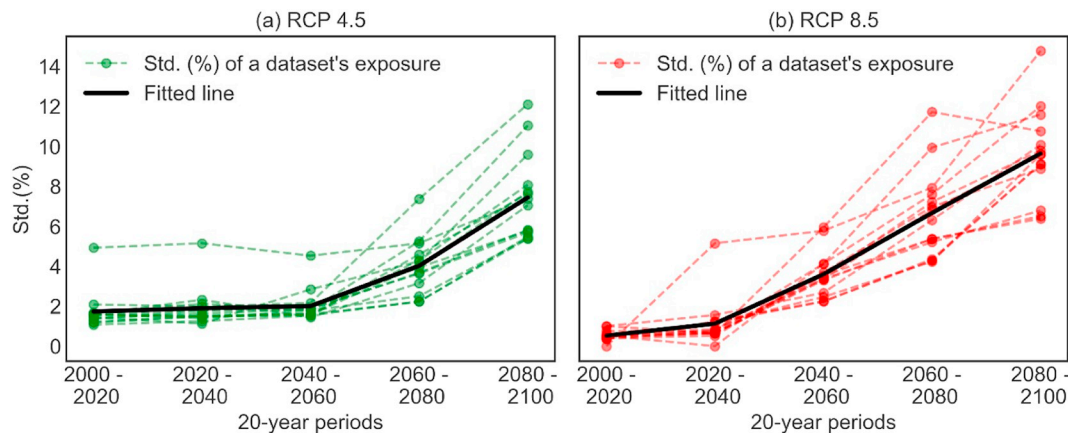
Fig. 8. Temporal trends of the uncertainties in the relative flood exposures of the fourteen datasets. (a) shows the uncertainties under RCP 4.5 scenarios. (b) shows the uncertainties under RCP 8.5 scenarios. The color dashed line shows the uncertainties in relative exposures of a dataset under a given RCP over time, whereas the solid black line shows the expected uncertainties. For a dataset, uncertainty is the standard deviation (Std.) of its relative exposures under a RCP and during a 20-year period. Expected uncertainty is predicted with the regression of Eq. (4).

periods, RCP 8.5 has smaller expected uncertainties than those of RCP 4.5, but this relationship inverts during the remaining periods.

The expected uncertainties in the dataset's relative exposures to different flood depths show varied temporal trends (i.e. based on the regression of Eq. (4)) (Fig. 9). Low to very high exposures (i.e. the max. flood depth < 2 m) show similar temporal trends with moderate increases in their uncertainties over time. However, extreme exposure (i.e. the max. flood depth > 2 m) has more distinct temporal trends with much larger uncertainties, particularly during the later periods such as those after 2080 for RCP 4.5 scenarios (Fig. 9(a)) and after 2060 for RCP 8.5 scenarios (Fig. 9(b)).

4. Discussions

4.1. Flood exposure under an uncertain future

Understanding flood exposure caused by SLR and storm surge is a prerequisite to obtain further information regarding risk, vulnerability, impact, resilience, and adaptation options in coastal urban areas under climate change. Projecting flood exposure involves a substantial amount of uncertainties that are propagated through a chain of

different political, socioeconomic and technological assumptions, GHG emissions and concentrations (i.e. the RCPs in this study), and climate models (i.e. the GCMs and probabilistic SLR values in this study) (Wilby & Dessai, 2010). Our results empirically show what the climate-related uncertainties would be like in a highly urbanized area, regarding the exposures of socioeconomic and demographic distributions, developed areas, lifeline infrastructures, and emergency responders to modeled flooding during extreme sea level events projected under two groups of climate scenarios (i.e. RCP 4.5 and 8.5), every 20 years between 2000 and 2100. We postulate that uncertainties should not be neglected, particularly for planning horizons beyond 2040 where our results indicate more salient uncertainties in relative exposures (Figs. 8 and 9).

Since flooding is sensitive to its underlying terrain conditions, coastal areas with flat terrain are more likely to experience uncertainties in projected flood exposures when compared with areas on steeper slopes. In flat areas, slight variations in projected sea levels can make the resulting flood areas advance or retreat over longer distances. For example, cities in the northeastern valleys of the Bay Area have more agreements in their flood areas between the low, median, and high estimates of the extreme sea level events (Fig. 10(a)). Alameda, a city built on flat landfill, is not only projected to have larger flood areas
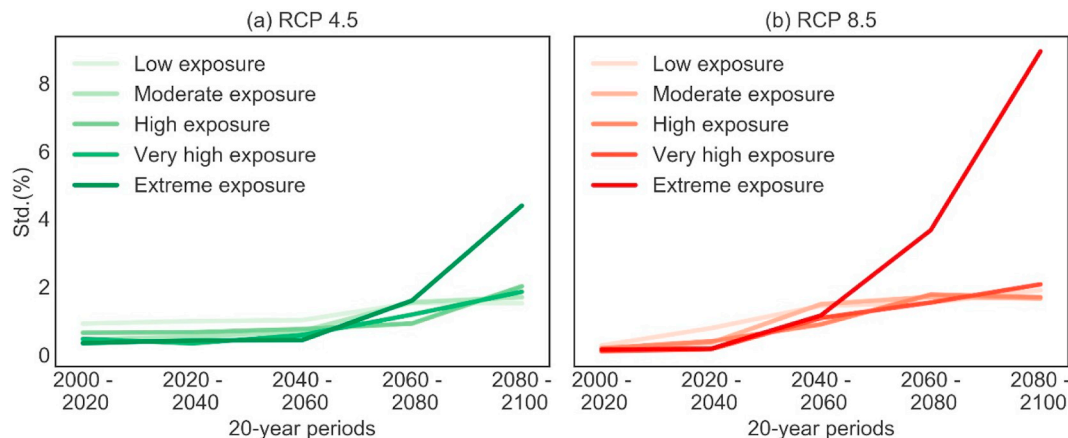

Fig. 9. Temporal trends of the expected uncertainties in the fourteen datasets' relative exposures to different flood depths. (a) the temporal trends under RCP 4.5, (b) the temporal trends under RCP 8.5.
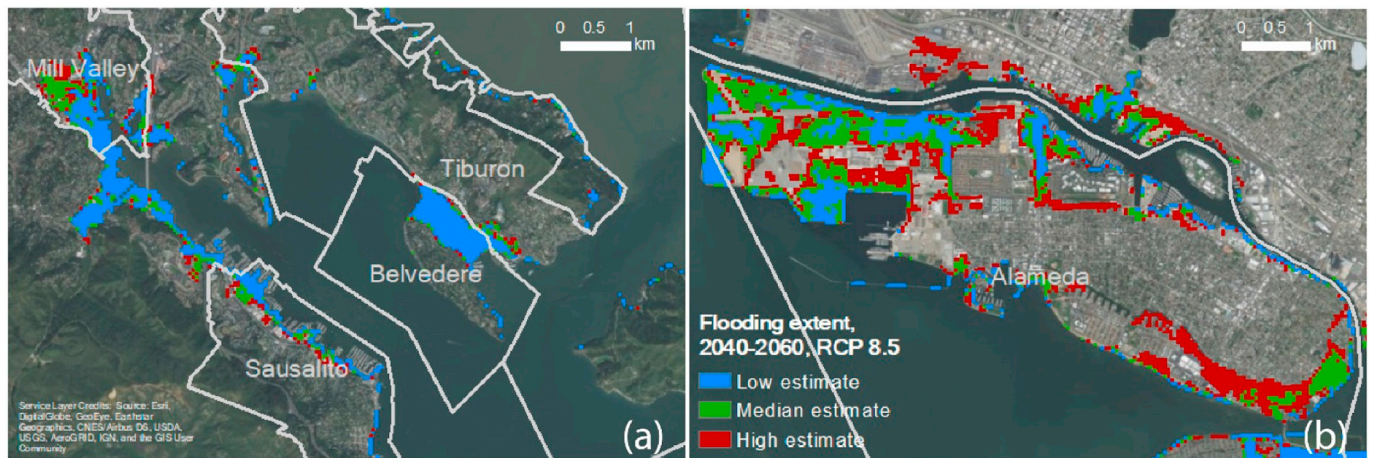
Fig. 10. Comparing high, median, and low estimates of flood areas in places with steep (a) and flat (b) terrain. This example is illustrated using extreme sea level events under the RCP 8.5 scenarios during the 2040–2060 period.

but also greater differences between the low, median and high estimates (Fig. 10(b)). Additional coastal developments are expected to emerge throughout the Bay Area due to the region's growing economy, projected increases in population and jobs, and amenities near the waterfront. A 2015 map found that 27 major proposed and ongoing real estate projects were located in flood-prone coastal zones (Wachtel, Ennamorato, & Burson, 2015) where the projected flood exposures were not only salient but also more uncertain, adding challenges to planning, management, and decision-making.

While we only highlight climate-related uncertainties in this study, non-climatic factors can also affect the uncertainties in projected flood hazards and exposures. These factors include land subsidence and uplift, different population distribution projections, land cover and land use changes, and improvements or failures of flood control structures. A recent model at 2 m spatial resolution (Shirzaei & Bürgmann, 2018) indicates that land subsidence and uplift will make flood areas increase from 51-168 km^2 to 98–218 km^2 by 2100 in the southern Bay Area under a likely range (i.e. 67% probability) of SLR scenarios. These land subsidence and uplift projections slightly (i.e. statistically insignificant) alter our results at 50 m resolution, causing flood areas within the southern Bay Area (the extent of this area is in Appendix C) to increase by 0.23 km^2 and the datasets' relative exposures to increase by 0.62% on average during the extreme sea level events. In addition, the uncertainties in flood areas decrease by 0.07 km^2, and the uncertainties in a dataset's exposures decrease by 0.31% on average under the two RCPs and during the five 20-year periods. However, all these changes are small and statistically insignificant, for two reasons. First, Shirzaei et al. only consider SLR and exclude extreme storm surge, whereas we include both phenomena. Therefore, compared with Shirzaei et al., our projected flood areas are more extensive and likely cover coastal regions with salient land subsidence, even without including this effect. Adding land subsidence to our models should not change projected flood area in these regions or the broader study area. Second, our 50 m spatial resolution and average aggregation may attenuate the effects of land subsidence and uplift. Given the sensitivity of flood models to spatial resolution (Haile & Rientjes, 2005; Jakovljević & Govedarica, 2019; Ju et al., 2017), we assume that models at a finer spatial resolution such as 2 m may lead to significant changes in flood exposures

and their uncertainties such as the ones observed by Shirzaei et al. These uncertainties may further increase when considering different land use and population projections, such as a recent Californian land use projection that contains four land use scenarios based on different population growth trajectories (Sleeter, Wilson, Sharygin, & Sherba, 2017). Levees are more relevant in low-lying and flat terrains, such as the adjacent Sacramento-San Joaquin River Delta whose islands are mostly 3–8 m below the current-day sea level (Ingebritsen, Ikehara, Galloway, & Jones, 2000) and protected by an extensive levee system (Mount & Twiss, 2005). These islands will likely be entirely flooded if the levees are overtopped or breached, and thus levee condition is a critical and uncertain factor for adaptation planning in this region. These non-climatic factors above, in addition to the climate drivers, serve to broaden the uncertainties in projected flood exposures.

4.2. Implications of the uncertainties for planning and management

To understand the implications of our results for planning and management in the Bay Area, we engaged with private and public stakeholders in the transportation and energy sectors. This outreach process is part of a broader project (Radke et al., 2018) that studies flood-related vulnerabilities of some lifeline infrastructures in our analysis. Two implications for planning and management are worth highlighting from this outreach process. First, the increased uncertainties over time pose obstacles for stakeholders to appreciate our long-term, multi-scenario flood projections and exposure analysis. Second, the obstacles above require adaptation strategies to cope with uncertainties and to promote long-term planning.

Concerns about uncertainties in long-term climate change projections and adaptations are not unique to the stakeholders we engaged with, they are also relevant for stakeholders in other sectors. Many of the stakeholders we interviewed are more interested in our near-term projections such as for 2000–2020 and 2020–2040, with insights from a few private-sector stakeholders suggesting that projections exceeding 10 years would be irrelevant in near-term decision making. This short-term focus is likely an uncertainty-avoidance organizational behavior (Slawinski, Pinkse, Busch, & Banerjee, 2017) that can be suboptimal in the long-term for infrastructures with longer investment, life, and

planning cycles (Hallegatte, 2009). Concerns about uncertainty have also been reported in other sectors such as public land management (Peters, Schwartz, & Lubell, 2018), urban planning (Carter et al., 2015), business firms (Slawinski et al., 2017), and public outreach (Morton, Rabinovich, Marshall, & Bretschneider, 2011). Since the negative consequences of future climate are not certain, stakeholders worry about losing predictability and control, and are inclined to keep self-interested behaviors, which may reduce the likelihood of taking actions for adaptation (Morton et al., 2011; Slawinski et al., 2017). This could explain the preference of stakeholders for short-term projections and exposure analysis that have smaller uncertainties as discovered in our results.

Based on our findings and from the existing literature, planning and management strategies should incorporate the uncertain nature of future climate and promote long-term thinking (Oddo et al., 2017; Walker, Haasnoot, & Kwakkel, 2013; Woodward, Kapelan, & Gouldby, 2014). Hallegatte (2009) recommends no-regret (i.e. beneficial even without climate change) and reversible (i.e. low cost for being wrong about future climate) adaptation strategies to cope with uncertainties. Additionally, uncertainty-coping strategies are not only technical but also "soft" by incorporating financial, organizational and institutional measures. Such strategies should enhance redundancy of a given system and enable decision-making in a timely manner to keep pace with new situations. Our outreach process with the stakeholders reveals preferences for technical and irreversible adaptation strategies such as armoring infrastructures and building levees. We also find some interest in no-regret and "soft" strategies including building mutual aid and self-sufficient logistic groups for emergency preparedness, which can be promoted as these strategies are assumed to be lower-cost and more flexible than the technical and irreversible ones when adjusting to new climate projections. Another salient example of 'soft' strategy that could be considered is the Sand Engine, a mega scale sand replenishment driven by waves and currents, implemented in the Netherlands to control for SLR-driven coastal recession while reducing project cost and disruptions to nature (Stive et al., 2013).

The long-term thinking is enhanced with the inclusion of certainties in climate change adaptation, such as adopting stable regulations over time that provide more predictability about future policy environment and reduce the risk of implementing certain adaptation actions (Slawinski et al., 2017). Furthermore, policies may explicitly require development projects to consider the long term. For example, a Bay Area's regulation has asked coastal projects to cope with flood projections for 2050 or 2100 depending on project life and existence of public safety risks (The San Francisco Bay Conservation and Development Commission, 2011). In realizing such long-term consideration, researchers, planners, and decision-makers may also utilize the concept of 'adaption tipping point' (Kwadijk et al., 2010), which is carried out in the Netherlands to identify the time points when current strategies are no longer valid due to climate change and when new strategies are need.

4.3. Limitations and future research directions

While we focus on exposure in this study, it does not equal to flood impacts on urban areas. Future researchers may acquire additional information to transform exposure into impact related metrics such as disruptions in traffic flows, damages to homes, and loss of life through damage-depth curves (Huizinga, de Moel, Szewczyk, European Commission, and Joint Research Centre, 2016; Pistrika, Tsakiris, &

Nalbantis, 2014). In addition to studying direct impacts in exposed areas, researchers may further consider a network framework where flood impacts can propagate through intra- or inter-connected infrastructures, spreading impacts over a much broader region (Biging et al., 2012; Ge, Dou, & Zhang, 2017). Researchers suggest that this network perspective provides a more holistic picture on flood impacts and their related uncertainties (Balijepalli & Oppong, 2014; Eleutério, Hattemer, & Rozan, 2013; Haimes, 2009; Herrera, Flannery, & Krimmer, 2017; International Transport Forum (ITF), 2017; Lleras-Echeverri & Sanchez-Silva, 2001; Martinson, 2017; O'Rourke, 2007; Rodríguez-Núñez & García-Palomares, 2014).

Researchers can also benefit from collaborating with stakeholders during the flood modeling process. While we mainly presented our results to the stakeholders responsible for some lifeline infrastructures, future studies may expand to other relevant industries and sectors, collecting their opinions on flood modeling. The differences in the stakeholder's reactions (e.g. the preferences for short versus long term projections) may indicate their varied priorities and concerns about flooding and climate change adaptation. Such knowledge can inform more relevant and applicable regulations and policies. Furthermore, stakeholder engagement can help to identify appropriate modeling strategies in terms of spatial resolution, time horizons, areas of interest, and metrics for projecting flood hazard, which will hopefully lead to more stakeholder-specific results (Wadey et al., 2015).

Finally, a long-term, fine resolution, and consistent flood mapping inventory will benefit flood modeling, exposure and impact assessments, and consequently stakeholders. Such an inventory is becoming increasingly possible with the advances in remote sensing (Pekel, Cottam, Gorelick, & Belward, 2016), sensor networks (Chang & Guo, 2006), and volunteered geographic information (Poser & Dransch, 2010). As more floods are monitored and mapped, flood models can be calibrated with this growing historical inventory, instead of water level recordings from sparse gauges used by this study. With such an inventory in place, researchers can use flood maps to develop statistical models, which can be better applied to large regions and used to compare with process-based models; like the 3Di used in this study (Siahkamari, Haghizadeh, Zeinivand, Tahmasebipour, & Rahmati, 2017; Tien Bui et al., 2016; Wang et al., 2015). Additionally, historical maps are intuitive tools that increase public awareness about flood hazards and are baselines to better understand variabilities in flood exposure and impact under future climates.

5. Conclusion

SLR and storm surge under climate change pose additional flood threats to coastal urban areas. Successful adaptation requires pro-active planning that incorporates long-term flood projections and their intrinsic uncertainties. While these intrinsic uncertainties are previously understudied, in this study we utilize a scalable hydrodynamic model to simulate coastal flooding under multiple time horizons and climate scenarios to show the range of flood exposures in a highly urbanized coastal area. We assess flood exposure by intersecting simulated flood areas with fourteen datasets describing demographic and socio-economic distributions, developed areas, lifeline infrastructures, and emergency responders. Our results are useful as a comprehensive base map for adaptation planning and to facilitate discussions with different stakeholders on adaptation options for future flood hazards while promoting transparency in the climate-related uncertainties associated. The approach we develop here can be used in coastal urban areas
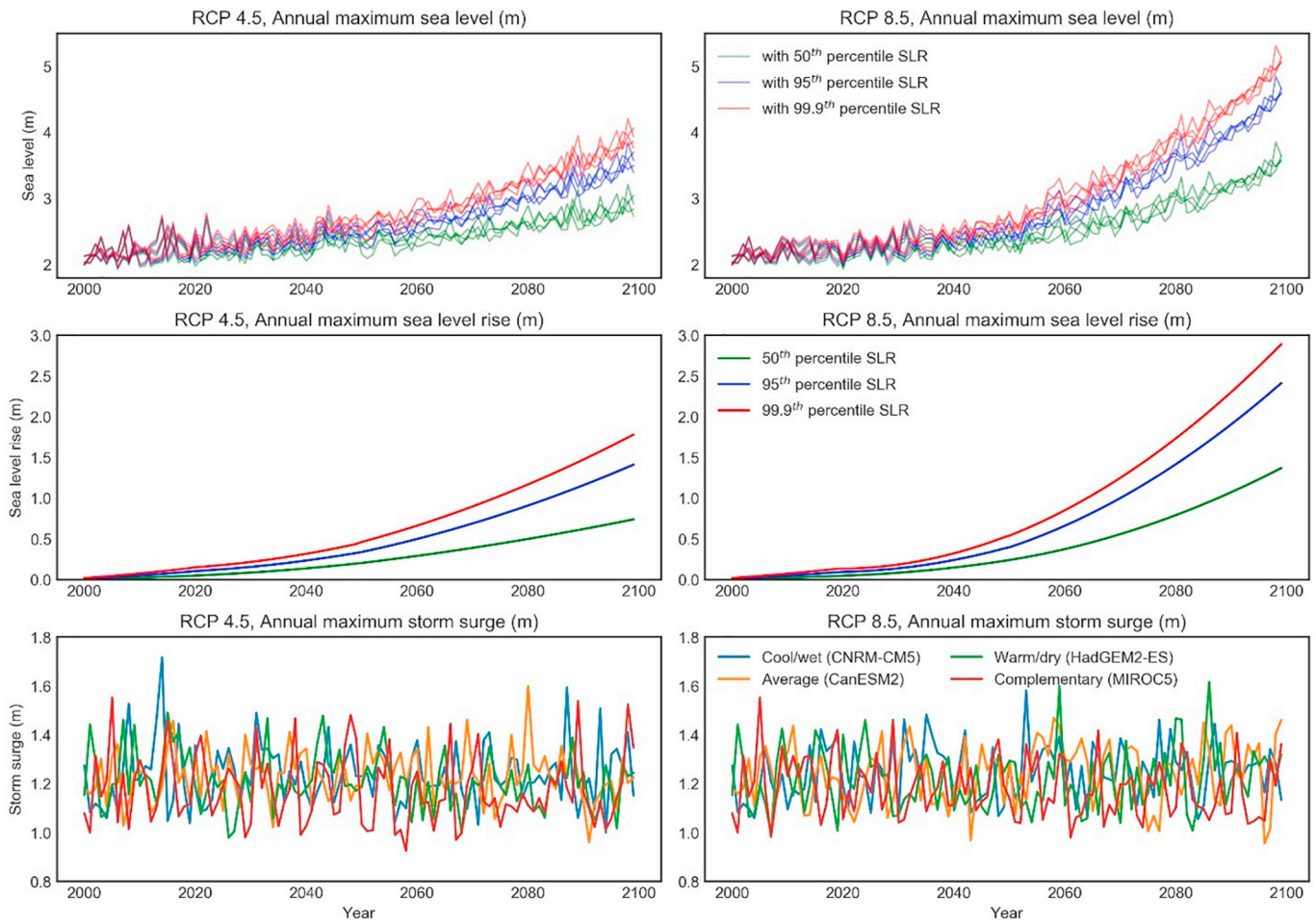
throughout the world.

Our results show increased flood exposures and broader uncertainties over time in the San Francisco Bay Area. The median estimates of lower GHG concentration scenarios (i.e. RCP 4.5) indicate 10–38% of the datasets' low-lying portions (i.e. < 10 m in elevation) are exposed to flood in 2000–2020 and 20–54% exposed in 2080–2100. These numbers change to 0–35% and 40–67% respectively under the median estimates of higher GHG concentration scenarios (i.e. RCP 8.5). The expected uncertainties (i.e. standard deviations) in a given dataset's exposures is 1–2% (RCP 8.5 and 4.5) in the 2000–2020 period and 7–10% (RCP 4.5 and 8.5) in the 2080–2100 period. We find that these increased uncertainties are challenging for stakeholders when using long-term projections, particularly for private-sector stakeholders who tend to focus on short-term investment and planning cycles. Therefore, adaptation options should favor no-regret, reversible, and redundant strategies, and policies should be stable over time. With such efforts, stakeholders are more likely to engage with flood and climate change adaptation.

Appendix A. Visualization of annual maximum value of the hourly sea level projections, SLR, and storm surge from Cayan et al. (2016)

Appendix B

B.1. Absolute exposures under RCP 4.5 and 8.5 scenarios, every 20 years between 2000 and 2100

Estimates	RCP 4.5			RCP 8.5		
	Min.	Median	Max.	Min.	Median	Max.
Period			2000–2020			
Population (1000 people)	163	195	233	156	162	164
Number of households (1000 households)	60	73	85	58	60	60

Number of housing units (1000 housing units)	63	77	90	62	63	64
High intensity development (km^2)	17	21	24	15	17	18
Medium intensity development (km^2)	50	56	61	45	49	50
Low intensity development (km^2)	41	45	48	38	41	41
Open space (km^2)	24	26	28	23	24	24
Roads (km)	1215	1393	1540	1095	1197	1225
Natural gas pipeline (km)	66	75	85	59	65	66
Natural gas stations (station)	6	6	8	5	6	6
Electric transmission line (km)	312	332	355	294	308	311
Electric substations (substation)	17	18	22	14	16	17
Fire stations (station)	13	17	17	10	13	13
Hospitals (hospital)	0	1	1	0	0	0
Period			2020–2040			
Population (1000 people)	143	195	200	163	189	208
Number of households (1000 households)	52	73	75	59	70	77
Number of housing units (1000 housing units)	55	77	80	63	74	82
High intensity development (km^2)	15	21	24	18	21	22
Medium intensity development (km^2)	46	56	61	51	56	57
Low intensity development (km^2)	39	45	47	42	45	45
Open space (km^2)	23	26	27	25	26	26
Roads (km)	1121	1404	1530	1245	1381	1426
Natural gas pipeline (km)	60	76	82	68	75	76
Natural gas stations (station)	6	6	8	6	6	6
Electric transmission line (km)	296	333	350	315	332	335
Electric substations (substation)	14	18	22	17	17	18
Fire stations (station)	11	17	17	13	17	17
Hospitals (hospital)	0	1	1	0	1	1
Period			2040–2060			
Population (1000 people)	178	193	229	173	214	256
Number of households (1000 households)	66	73	83	63	75	90
Number of housing units (1000 housing units)	70	77	88	67	80	95
High intensity development (km^2)	20	23	28	18	29	41
Medium intensity development (km^2)	53	59	67	52	69	86
Low intensity development (km^2)	44	46	50	43	52	57
Open space (km^2)	25	27	29	25	30	33
Roads (km)	1314	1475	1703	1268	1762	2267
Natural gas pipeline (km)	71	79	94	68	101	136
Natural gas stations (station)	6	6	10	6	10	13
Electric transmission line (km)	323	343	372	317	383	429
Electric substations (substation)	17	21	23	17	26	38
Fire stations (station)	15	17	19	14	20	23
Hospitals (hospital)	0	1	1	0	1	2
Period			2060–2080			
Population (1000 people)	219	262	244	236	288	381
Number of households (1000 households)	79	92	89	83	107	138
Number of housing units (1000 housing units)	84	98	95	87	113	147
High intensity development (km^2)	24	34	45	28	56	70
Medium intensity development (km^2)	60	76	90	68	104	124
Low intensity development (km^2)	48	54	59	51	63	69
Open space (km^2)	28	32	34	30	37	40
Roads (km)	1509	1970	2393	1730	2793	3338
Natural gas pipeline (km)	83	115	144	97	168	199
Natural gas stations (station)	8	12	12	10	15	23
Electric transmission line (km)	353	402	441	376	475	519
Electric substations (substation)	22	32	41	24	49	58
Fire stations (station)	17	21	24	19	28	36
Hospitals (hospital)	1	1	2	1	2	3
Period			2080–2100			
Population (1000 people)	203	279	414	277	483	546
Number of households (1000 households)	72	101	151	103	172	199
Number of housing units (1000 housing units)	76	108	163	109	183	214
High intensity development (km^2)	28	59	77	54	87	100
Medium intensity development (km^2)	68	108	134	102	151	175
Low intensity development (km^2)	51	64	72	62	77	84
Open space (km^2)	30	37	42	36	44	48
Roads (km)	1736	2906	3634	2747	4129	4784
Natural gas pipeline (km)	98	174	218	165	243	286
Natural gas stations (station)	10	17	26	15	27	32
Electric transmission line (km)	380	485	544	470	584	624
Electric substations (substation)	25	51	63	49	70	77
Fire stations (station)	19	30	38	28	45	51
Hospitals (hospital)	1	2	3	2	5	5

B.2. Total amount of each dataset used in the exposure analysis

Dataset	Total amount	Dataset	Total amount
Population (1000 people)	1153	Roads (km)	8160
Number of households (1000 households)	430	Natural gas pipeline (km)	531
Number of housing units (1000 housing units)	464	Natural gas stations (station)	55
High intensity development (km^2)	155	Electric transmission line (km)	967
Medium intensity development (km^2)	296	Electric substations (substation)	105
Low intensity development (km^2)	125	Fire stations (station)	95
Open space (km^2)	69	Hospitals (hospital)	10

Appendix C. Area of the analysis with land subsidence and uplift data

References

Balijepalli, C., & Oppong, O. (2014). Measuring vulnerability of road network considering the extent of serviceability of critical road links in urban areas. *Journal of Transport Geography, 39*, 145–155. https://doi.org/10.1016/j.jtrangeo.2014.06.025.

Barnard, P. L., O'Reilly, B., van Ormondt, M., Elias, E., Ruggiero, P., Erikson, L. H., ... Adams, P. N. (2009). *The framework of a coastal hazards model - a tool for predicting the impact of severe storms. U. S. Geological Survey.*

Barnard, P. L., van Ormondt, M., Erikson, L. H., Eshleman, J., Hapke, C., Ruggiero, P., ... Foxgrover, A. C. (2014). Development of the Coastal Storm Modeling System (CoSMoS) for predicting the impact of storms on high-energy, active-margin coasts. Natural Hazards, 74(2), 1095–1125. https://doi.org/https://doi.org/10.1007/s11069-014-1236-y.

Bickers, K. M. (2014). *Vulnerable populations to climate change in New Jersey. Edward J. Bloustein School of Planning and Public Policy Rutgers, The State University of New Jersey Rutgers University.*

Biging, G., Radke, J., & Lee, J. H. (2012). *Impacts of predicted sea-level rise and extreme storm events on the transportation in the San Francisco Bay Region (No. CEC - 500 - 2012 - 040). California Energy Commission.*

Carter, J. G., Cavan, G., Connelly, A., Guy, S., Handley, J., & Kazmierczak, A. (2015). Climate change and the city: Building capacity for urban adaptation. *Progress in Planning, 95*, 1–66. https://doi.org/10.1016/j.progress.2013.08.001.

Cayan, D. R., Kalansky, J., Iacobellis, S., & Pierce, D. (2016). *Creating probabilistic sea leve rise projections to support the 4th California Climate Assessment* (No. 16- IEPR- 04). Retrieved from California Energy Commissionhttp://docketpublic.energy.ca.gov/PublicDocuments/16-IEPR-04/TN211806_20160614T101823_Creating_Probabilistic_Sea_Leve_Rise_Projections.pdf.

Chang, N.-B., & Guo, D.-H. (2006). Urban flash flood monitoring, mapping and forecasting via a tailored sensor network system. In 2006 IEEE International Conference on Networking, Sensing and Control (pp. 757–761). https://doi.org/https://doi.org/10.1109/ICNSC.2006.1673241.

Coles, D., Yu, D., Wilby, R. L., Green, D., & Herring, Z. (2017). Beyond 'flood hotspots': Modelling emergency service accessibility during flooding in York, UK. *Journal of Hydrology, 546*, 419–436. https://doi.org/10.1016/j.jhydrol.2016.12.013.

Creel, L. (2003). *Ripple effects: Population and coastal regions. Washington, DC: Population Reference Bureau.*

Dahm, R., Hsu, C.-T., Lien, H.-C., Chang, C.-H., & Prinsen, G. (2014). *Next generation flood modelling using 3Di: A case study in Taiwan. Presented at the DSD international conference 2014, sustainable stormwater and waste water management, Hong Kong.*

Dasgupta, S., Laplante, B., Meisner, C., Wheeler, D., & Yan, J. (2008). The impact of sea level rise on developing countries: A comparative analysis. *Climatic Change, 93*(3–4), 379–388. https://doi.org/10.1007/s10584-008-9499-5.

Dawson, R. J., Ball, T., Werritty, J., Werritty, A., Hall, J. W., & Roche, N. (2011). Assessing the effectiveness of non-structural flood management measures in the Thames Estuary under conditions of socio-economic and environmental change. *Global Environmental Change, 21*(2), 628–646. https://doi.org/10.1016/j.gloenvcha.2011.01.013.

De Sherbinin, A., Schiller, A., & Pulsipher, A. (2007). The vulnerability of global cities to climate hazards. *Environment and Urbanization, 19*(1), 39–64. https://doi.org/10.1177/0956247807076725.

Demirel, H., Kompil, M., & Nemry, F. (2015). A framework to analyze the vulnerability of European road networks due to Sea-Level Rise (SLR) and sea storm surges. Transportation Research Part A: Policy and Practice, 81, 62–76. https://doi.org/https://doi.org/10.1016/j.tra.2015.05.002.

EERI (2016). *Improve Reliability of Lifeline Infrastructure Systems* (Policy White Paper). Oakland, CA: Earthquake Engineering Research Institute. Retrieved from https://www.eeri.org/wp-content/uploads/eeri-policy-lifelines.pdf.

Eleutério, J., Hattemer, C., & Rozan, A. (2013). A systemic method for evaluating the potential impacts of floods on network infrastructures. *Natural Hazards and Earth System Science, 13*(4), 983–998. https://doi.org/10.5194/nhess-13-983-2013.

ESRI (2016). *ArcGIS Desktop (Version 10.4). ArcMap 10.4: ESRI.*

Ge, Y., Dou, W., & Zhang, H. (2017). A new framework for understanding urban social vulnerability from a network perspective. *Sustainability, 9*(10), 1723. https://doi.org/10.3390/su9101723.

Haile, A. T., & Rientjes, T. H. M. (2005). Effects of LiDAR DEM resolution in flood modelling: A model sensitivity study for the city of Tegucigalpa, Honduras. *Isprs Wg Iii/3, Iii/4. Vol. 3. Isprs Wg Iii/3, Iii/4* (pp. 12–14).

Haimes, Y. Y. (2009). On the complex definition of risk: A systems-based approach. *Risk Analysis, 29*(12), 1647–1654. https://doi.org/10.1111/j.1539-6924.2009.01310.x.

Hallegatte, S. (2009). Strategies to adapt to an uncertain climate change. *Global Environmental Change, 19*(2), 240–247. https://doi.org/10.1016/j.gloenvcha.2008.12.003.

Heberger, M., Cooley, H., Moore, E., & Herrera, P. (2012). *The impacts of sea level rise on the San Francisco Bay (No. CEC - 500 - 2012 - 014). California Energy Commission.*

Herrera, E. K., Flannery, A., & Krimmer, M. (2017). Risk and resilience analysis for highway assets. *Transportation Research Record: Journal of the Transportation Research Board, 2604*(1), 1–8. https://doi.org/10.3141/2604-01.

Hsu, Y.-C., Prinsen, G., Bouaziz, L., Lin, Y.-J., & Dahm, R. (2016). An investigation of DEM resolution influence on flood inundation simulation. *Procedia Engineering, 154*, 826–834. https://doi.org/10.1016/j.proeng.2016.07.435.

Huizinga, J., de Moel, H., Szewczyk, W., European Commission, & Joint Research Centre (2016). *Global flood depth-damage functions methodology and the database with guidelines. Luxembourg: Publications Office.*

Hunt, A., & Watkiss, P. (2010). Climate change impacts and adaptation in cities: A review of the literature. *Climatic Change, 104*(1), 13–49. https://doi.org/10.1007/s10584-

010-9975-6.

Ingebritsen, S. E., Ikehara, M. E., Galloway, D. L., & Jones, D. R. (2000). *Delta subsidence in California; the sinking heart of the state* (No. Fact Sheet 005-00). Retrieved from U.S. Geological Surveyhttp://pubs.usgs.gov/fs/2000/fs00500/.

International Transport Forum (ITF) (2017). Adapting transport to climate change and extreme weather: Implications for infrastructure owners and network managers. Paris: ITF Research Reports, OECD. Retrieved from https://doi.org/10.1787/9789282108079-en.

Jabareen, Y. (2015). City planning deficiencies & climate change – The situation in developed and developing cities. *Geoforum, 63*, 40–43. https://doi.org/10.1016/j.geoforum.2015.05.017.

Jakovljević, G., & Govedarica, M. (2019). Water body extraction and flood risk assessment using Lidar and open data. In W. Leal Filho, G. Trbic, & D. Filipovic (Eds.), Climate change adaptation in Eastern Europe: Managing risks and building resilience to climate change (pp. 93–111). Cham: Springer International Publishing. https://doi.org/https://doi.org/10.1007/978-3-030-03383-5_7.

Ju, Y., Hsu, W.-C., Radke, J., Fourt, W., Lang, W., Hoes, O., ... Maier, W. (2017). Planning for the change: Mapping sea level rise and storm inundation in Sherman Island using 3Di hydrodynamic model and LiDAR. In P. (Vonu) Thakuriah, N. Tilahun, & M. Zellner (Eds.), Seeing cities through big data (pp. 313–329). Springer International Publishing. https://doi.org/https://doi.org/10.1007/978-3-319-40902-3_18.

Kaźmierczak, A., & Cavan, G. (2011). Surface water flooding risk to urban communities: Analysis of vulnerability, hazard and exposure. *Landscape and Urban Planning, 103*(2), 185–197. https://doi.org/10.1016/j.landurbplan.2011.07.008.

KC, B., Shepherd, J. M., & Gaither, C. J. (2015). Climate change vulnerability assessment in Georgia. *Applied Geography, 62*, 62–74. https://doi.org/10.1016/j.apgeog.2015.04.007.

Knowles, N. (2009). *Potential inundation due to rising sea levels in the San Francisco Bay Region* (No. CEC-500-2009-023-D). Retrieved from California Climate Change Centerhttp://www.energy.ca.gov/2009publications/CEC-500-2009-023/CEC-500-2009-023-D.PDF.

Knowles, N. (2010). Potential inundation due to rising sea levels in the San Francisco Bay Region. *San Francisco Estuary and Watershed Science, 8*(1), Retrieved from http://escholarship.org/uc/item/8ck5h3qn.

Kwadijk, J. C. J., Haasnoot, M., Mulder, J. P. M., Hoogvliet, M. M. C., Jeuken, A. B. M., van der Krogt, R. A. A., ... de Wit, M. J. M. (2010). Using adaptation tipping points to prepare for climate change and sea level rise: A case study in the Netherlands. Wiley Interdisciplinary Reviews: Climate Change, 1(5), 729–740. https://doi.org/https://doi.org/10.1002/wcc.64.

Lang, W., Radke, J. D., Chen, T., & Chan, E. H. W. (2016). Will affordability policy transcend climate change? A new lens to re-examine equitable access to healthcare in the San Francisco Bay Area. *Cities, 58*, 124–136. https://doi.org/10.1016/j.cities.2016.05.014.

Leicher, A. M. (2016). *Urban flood analyses in sloping areas with 3Di modelling.*

Lleras-Echeverri, G., & Sanchez-Silva, M. (2001). Vulnerability analysis of highway networks, methodology and case study. *Proceedings of the Institution of Civil Engineers, Transport, 147*(4), 223–236.

Marcy, D., Herold, N., Waters, K., Brooks, W., Hadley, B., Pendleton, M., ... Ryan, S. (2011). *New mapping tool and techniques for visualizing Sea Level Rise and coastal flooding impacts. NOAA Coastal Service Center.*

Martinich, J., Neumann, J., Ludwig, L., & Jantarasami, L. (2013). Risks of sea level rise to disadvantaged communities in the United States. *Mitigation and Adaptation Strategies for Global Change, 18*(2), 169–185. https://doi.org/10.1007/s11027-011-9356-0.

Martinson, R. (2017). Resilience in a transportation system: A whole system approach. *Transportation Research Circular, (Circular E-226)* (pp. 1–9). .

McGranahan, G., Balk, D., & Anderson, B. (2007). The rising tide: Assessing the risks of climate change and human settlements in low elevation coastal zones. *Environment and Urbanization, 19*(1), 17–37. https://doi.org/10.1177/0956247807076960.

Morton, T. A., Rabinovich, A., Marshall, D., & Bretschneider, P. (2011). The future that may (or may not) come: How framing changes responses to uncertainty in climate change communications. *Global Environmental Change, 21*(1), 103–109. https://doi.org/10.1016/j.gloenvcha.2010.09.013.

Moss, R. H., Edmonds, J. A., Hibbard, K. A., Manning, M. R., Rose, S. K., ... van Vuuren, D. P., Wilbanks, T. J. (2010). The next generation of scenarios for climate change research and assessment. *Nature, 463*(7282), 747–756.

Mount, J., & Twiss, R. (2005). Subsidence, sea level rise, and seismicity in the Sacramento–San Joaquin Delta. *San Francisco Estuary and Watershed Science, 3*(1), Retrieved from http://escholarship.org/uc/item/4k44725p.

Neumann, B., Vafeidis, A. T., Zimmermann, J., & Nicholls, R. J. (2015). Future coastal population growth and exposure to sea-level rise and coastal flooding - A global assessment. *PLoS One, 10*(3), e0118571. https://doi.org/10.1371/journal.pone.0118571.

NOAA (2019). Water levels - NOAA tides & currents. Retrieved March 20, 2019, from https://tidesandcurrents.noaa.gov/waterlevels.html?id=9414290.

Nutters, H. (2012). *Addressing social vulnerability and equity in climate change adaptation planning. San Francisco Bay Conservation and Development Commission.*

Oddo, P. C., Lee, B. S., Garner, G. G., Srikrishnan, V., Reed, P. M., Forest, C. E., & Keller, K. (2017). Deep uncertainties in sea-level rise and storm surge projections: Implications for coastal flood risk management: Deep uncertainties in coastal flood risk management. *Risk Analysis*, 1–16. https://doi.org/10.1111/risa.12888.

Oh Eun Ho, Deshmukh Abhijeet, & Hastak Makarand. (2013). Criticality assessment of lifeline infrastructure for enhancing disaster response. Natural Hazards Review, 14(2), 98–107. https://doi.org/10.1061/(ASCE)NH.1527-6996.0000084.

O'Rourke, T. D. (2007). *Critical Infrastructure, Interdependencies, and Resilience. Vol. 8.*

Pekel, J.-F., Cottam, A., Gorelick, N., & Belward, A. S. (2016). High-resolution mapping of global surface water and its long-term changes. *Nature, 540*(7633), 418–422. https://

doi.org/10.1038/nature20584.

Pelling, M. (2003). *The vulnerability of cities. [electronic resource]: Natural disasters and social resilience. 2003*Sterling, Va.: Earthscan Publications. Retrieved from http:// search.ebscohost.com/login.aspx?direct=true&db=cat04202a&AN=ucb. b13633897&site=eds-live.

Peters, C. B., Schwartz, M. W., & Lubell, M. N. (2018). Identifying climate risk perceptions, information needs, and barriers to information exchange among public land managers. Science of the Total Environment, 616–617, 245–254. https://doi.org/ https://doi.org/10.1016/j.scitotenv.2017.11.015.

Pierce, D., Cayan, D. R., & Dehann, L. (2016). *Creating climate projections to support the 4th California Climate Assessment* (No. 16- IEPR- 04). Retrieved from California Energy Commissionhttp://www.energy.ca.gov/2016_energypolicy/documents/2016-06-21_ workshop/2016-06-21_documents.php.

Pinto, P. J., & Kondolf, G. M. (2016). Evolution of two urbanized estuaries: Environmental change, legal framework, and implications for sea-level rise vulnerability. *Water, 8*(11), 535. https://doi.org/10.3390/w8110535.

Pistrika, A., Tsakiris, G., & Nalbantis, I. (2014). Flood depth-damage functions for built environment. *Environmental Processes, 1*(4), 553–572. https://doi.org/10.1007/ s40710-014-0038-2.

Poser, K., & Dransch, D. (2010). Volunteered geographic information for disaster management with application to rapid flood damage estimation. *Geomatica, 64*(1), 89–98.

Radke, J., Biging, G., Roberts, K., Foster, H., Roe, E., Ju, Y., ... Dalal, A. (2018). *Assessing extreme weather-related vulnerability and identifying resilience options for California's interdependent transportation fuel sector (California's Fourth Climate Change Assessment no. CCCA4- CEC-2018–012).* California Energy Commission. Retrieved from http:// www.climateassessment.ca.gov/techreports/docs/20180827-Energy_CCCA4-CEC- 2018-012.pdf.

Radke, J., Biging, G., Schimidt-Poolman, M., Foster, H., Roe, E., Ju, Y., ... Reeves, I. (2017). *Assessment of bay area gas pipeline vulnerability to climate change* (no. CEC-500- 2017-008). Retrieved from California Energy Commissionhttps://www.energy.ca. gov/2017publications/CEC-500-2017-008/CEC-500-2017-008.pdf.

Rodríguez-Núñez, E., & García-Palomares, J. C. (2014). Measuring the vulnerability of public transport networks. *Journal of Transport Geography, 35*, 50–63. https://doi. org/10.1016/j.jtrangeo.2014.01.008.

Rosenzweig, C., Solecki, W., Hammer, S. A., & Mehrotra, S. (2010). Cities lead the way in climate-change action. *Nature, 467*(7318), 909–911. https://doi.org/10.1038/ 467909a.

Schile, L. M., Callaway, J. C., Morris, J. T., Stralberg, D., Parker, V. T., & Kelly, M. (2014). Modeling tidal marsh distribution with sea-level rise: Evaluating the role of vegetation, sediment, and upland habitat in marsh resiliency. *PLoS One, 9*(2), e88760. https://doi.org/10.1371/journal.pone.0088760.

Seto, K. C., Fragkias, M., Güneralp, B., & Reilly, M. K. (2011). A meta-analysis of global urban land expansion. *PLoS One, 6*(8), e23777. https://doi.org/10.1371/journal. pone.0023777.

Shirzaei, M., & Bürgmann, R. (2018). Global climate change and local land subsidence exacerbate inundation risk to the San Francisco Bay Area. Science Advances, 4(3), eaap9234. https://doi.org/https://doi.org/10.1126/sciadv.aap9234.

Siahkamari, S., Haghizadeh, A., Zeinivand, H., Tahmasebipour, N., & Rahmati, O. (2017). Spatial prediction of flood-susceptible areas using frequency ratio and maximum entropy models. Geocarto International, 0(0), 1–15. https://doi.org/https://doi.org/ 10.1080/10106049.2017.1316780.

Slawinski, N., Pinkse, J., Busch, T., & Banerjee, S. B. (2017). The role of short-termism and uncertainty avoidance in organizational inaction on climate change: A multi-level framework. *Business & Society, 56*(2), 253–282. https://doi.org/10.1177/

0007650315576136.

Sleeter, B. M., Wilson, T. S., Sharygin, E., & Sherba, J. T. (2017). Future scenarios of land change based on empirical data and demographic trends: Land use projections for California. Earth's Future. https://doi.org/https://doi.org/10.1002/2015EF000560.

Stelling, G. S. (2012). Quadtree flood simulations with sub-grid digital elevation models. Proceedings of the ICE - Water Management, 165(10), 567–580. https://doi.org/ https://doi.org/10.1680/wama.12.00018.

Stive, M. J. F., de Schipper, M. A., Luijendijk, A. P., Aarninkhof, S. G. J., van Gelder-Maas, C., van Thiel de Vries, J. S. M., ... Ranasinghe, R. (2013). A new alternative to saving our beaches from sea-level rise: The sand engine. Journal of Coastal Research, 1001–1008. https://doi.org/https://doi.org/10.2112/JCOASTRES-D-13-00070.1.

Storch, H., & Downes, N. K. (2011). A scenario-based approach to assess Ho Chi Minh City's urban development strategies against the impact of climate change. *Cities, 28*(6), 517–526. https://doi.org/10.1016/j.cities.2011.07.002.

Strauss, B. H., Ziemlinski, R., Weiss, J. L., & Overpeck, J. T. (2012). Tidally adjusted estimates of topographic vulnerability to sea level rise and flooding for the contiguous United States. *Environmental Research Letters, 7*(1), 014033. https://doi.org/ 10.1088/1748-9326/7/1/014033.

The Association of Bay Area Governments (ABAG), & Metropolitan Transportation Commission (MTC) (2013). *Plan bay area: Strategy for a sustainable region*.

The San Francisco Bay Conservation and Development Commission (2011). SFBCDC - New Sea level rise policies fact sheet. Retrieved from http://www.bcdc.ca.gov/BPA/ SLRfactSheet.html.

Tien Bui, D., Pradhan, B., Nampak, H., Bui, Q.-T., Tran, Q.-A., & Nguyen, Q.-P. (2016). Hybrid artificial intelligence approach based on neural fuzzy inference model and metaheuristic optimization for flood susceptibility modeling in a high-frequency tropical cyclone area using GIS. *Journal of Hydrology, 540*, 317–330. https://doi.org/ 10.1016/j.jhydrol.2016.06.027.

UNU-IHDP (2015). *Coastal zones and urbanization. Summary for decision-makers.* Bonn: UNU-IHDP.

Wachtel, M., Ennamorato, M., & Burson, B. (2015). A baywide building boom threatened by rising waters. Berkeley, California: UC Berkeley CAGE Lab. Retrieved from http:// sfpublicpress.org/news/searise/2015-07/interactive-map-a-baywide-building-boom- threatened-by-rising-waters.

Wadey, M. P., Cope, S. N., Nicholls, R. J., McHugh, K., Grewcock, G., & Mason, T. (2015). Coastal flood analysis and visualization for a small town. *Ocean & Coastal Management, 116*, 237–247. https://doi.org/10.1016/j.ocecoaman.2015.07.028.

Walker, W., Haasnoot, M., & Kwakkel, J. (2013). Adapt or perish: A review of planning approaches for adaptation under deep uncertainty. *Sustainability, 5*(3), 955–979. https://doi.org/10.3390/su5030955.

Wang, Z., Lai, C., Chen, X., Yang, B., Zhao, S., & Bai, X. (2015). Flood hazard risk assessment model based on random forest. Journal of Hydrology, 527(Supplement C), 1130–1141. https://doi.org/https://doi.org/10.1016/j.jhydrol.2015.06.008.

Wilby, R. L., & Dessai, S. (2010). Robust adaptation to climate change. *Weather, 65*(7), 180–185. https://doi.org/10.1002/wea.543.

Wood, N. (2009). Tsunami exposure estimation with land-cover data: Oregon and the Cascadia subduction zone. *Applied Geography, 29*(2), 158–170. https://doi.org/10. 1016/j.apgeog.2008.08.009.

Woodward, M., Kapelan, Z., & Gouldby, B. (2014). Adaptive flood risk management under climate change uncertainty using real options and optimization: Adaptive flood risk management. *Risk Analysis, 34*(1), 75–92. https://doi.org/10.1111/risa.12088.

Zhu, M., Xi, X., Hoctor, T. S., & Volk, M. (2015). Integrating conservation costs into sea level rise adaptive conservation prioritization. *Global Ecology and Conservation, 4*, 48–62. https://doi.org/10.1016/j.gecco.2015.05.007.